Current Optics and Photonics
Vol. 1, No. 1, February 2017, pp. 17-22

ISSN: 2508-7266(Print) / ISSN: 2508-7274(Online)
DOI: https://doi.org/10.3807/COPP.2017.1.1.017

Stiffness Comparison of Tissue Phantoms using Optical Coherence Elastography without a Load Cell

Yu-Gyeong Chae[1], Eun-Kee Park[2,3], Min Yong Jeon[4], Byeong-Hwan Jeon[5], and Yeh-Chan Ahn[2,6,7]*

[1]*Medical Device Development Center, Osong Medical Innovation Foundation, Cheongju 28160 Korea.*
[2]*Innovative Biomedical Technology Research Center, Busan 49104 Korea*
[3]*Department of Medical Humanities and Social Medicine, Kosin University, Busan 49104, Korea*
[4]*Department of Physics, Chung Nam National University, Daejeon 34134, Korea*
[5]*School of Sports and Health, Kyungsung University, Busan 48434, Korea*
[6]*Department of Biomedical Engineering and Center for Marine-Integrated Biomedical Technology, Pukyong National University, Busan 48513, Korea*
[7]*Department of Interdisciplinary Program of Biomedical Mechanical and Electrical Engineering, Pukyong National University, Busan 48513, Korea*

(Received September 7, 2016 : revised November 6, 2016 : accepted January 5, 2017)

Mechanical property of tissue is closely related to diseases such as breast cancer, prostate cancer, cirrhosis of the liver, and atherosclerosis. Therefore measurement of tissue mechanical property is important for a better diagnosis. Ultrasound elastography has been developed as a diagnostic modality for a number of diseases that maps mechanical property of tissue. Optical coherence elastography (OCE) has a higher spatial resolution than ultrasound elastography. OCE, therefore, could be a great help for early diagnosis. In this study, we made tissue phantoms and measured their compressive moduli with a rheometer measuring the response to applied force. Uniaxial strain of the tissue phantom was also measured with OCE by using cross-correlation of speckles and compared with the results from the rheometer. In order to compare stiffness of tissue phantoms by OCE, the applied force should be measured in addition to the strain. We, however, did not use a load cell that directly measures the applied force for each sample. Instead, we utilized one silicone film (called as reference phantom) for all OCE measurements that indirectly indicated the amount of the applied force by deformation. Therefore, all measurements were based on displacement, which was natural and effective for image-based elastography such as OCE.

Keywords : Mechanical Property, Optical coherence tomography, Optical coherence elastography, Tissue phantom
OCIS codes : (110.4500) Optical coherence tomography, (120.3930) Metrological instrumentation

I. INTRODUCTION

Change of tissue mechanical property is closely related to progress of disease and can be used as a diagnostic contrast for breast cancer, prostate cancer, and liver cirrhosis [1]. Elastography has been developed and demonstrated improvement in diagnostic potential since it provides functional images in addition to structural information. The usefulness of ultrasound elastography and magnetic resonance elastography has been shown in clinical studies [2, 3].

Optical coherence elastography (OCE) [1, 4] is based on optical coherence tomography (OCT) that provides a cross-sectional view of tissue microstructure with a high-spatial resolution and a high-acquisition speed. As the technology of optical coherence tomography advances rapidly, OCE research field also grows continuously. Especially, OCE can be proposed as a diagnostic modality in an early stage from the mechanical aspect because it has a higher spatial

*Corresponding author: ahny@pknu.ac.kr
Color versions of one or more of the figures in this paper are available online.

resolution than other elastographic modalities.

OCE has a loading system that applies a force to a sample with unknown mechanical properties. Local response (it is also known as elastogram representing strain, phase velocity, natural frequency, or resonant vibration amplitude) to the loading is, then, imaged by OCT. Loading methods may include uniaxial compression, surface acoustic wave, shear wave, magnetomotive force, and frequency-swept loading [5]. From the relation between loading and local response, OCE estimates the relative stiffness of the sample related to Young's modulus or shear modulus. The Young's modulus cannot be calculated without knowing the local stress corresponding to the local strain. In principle, local stresses can be measured at the surface of the sample, but there is no known method for directly measuring the stresses in the sample. An indirect approach is possible to match the measured local strain with predictions based on the assumed stress distribution (called as the inverse method) [6].

In this study, we made a simple uniaxial compression with a piezoelectric actuator and uniaxial strain of the sample was measured with OCE by using cross-correlation of speckles. For an isotropic linear elastic material, compressive stress (σ) is proportional to strain (ε) where Young's modulus (or compressive modulus, Y) is the proportional constant as shown in Eq. (1). The compressive stress is defined as compressive force (F) divided by cross-sectional area (A) of the sample. Note that here we assume uniaxial uniform stress. The strain is defined as displacement (Δz) along depth divided by length (z) along depth.

$$\sigma = Y\varepsilon \tag{1}$$

where

$$\sigma = F/A \tag{2}$$

$$\varepsilon = \Delta z/z \tag{3}$$

A load cell is a transducer that is used to measure the applied force. The force exerted on biological sample is usually small (~ 1 N) for OCE and it should be measured by the load cell with a good accuracy (< 0.1 N) [5]. OCE, therefore, has to use not only a loading mechanism but also a sensitive load cell to measure the applied force for sample-to-sample stiffness comparison. In this study, however, any load cell was not used. Instead, we proposed a low cost silicone film (called as reference phantom) that indirectly indicated the amount of the applied force by deformation. After all, we only need to measure the displacement without measuring the force. Note that OCE is an image-based measurement technology that accurately measures the displacement.

II. METHODS

2.1 Optical coherence tomography setup

OCT is a high-resolution and non-invasive imaging technique based on the Michelson interferometer [7]. Since the development of spectral-domain OCT, it has been widely used for diagnosis of disease in early stage. We designed a 1310 nm k-linear spectral-domain OCT system (Fig. 1) [8]. Broadband light from a SLED light source (1310 nm SLED with a bandwidth of 80 nm, EXALOS, Schlieren, Switzerland) was guided using an optical fiber to a 50:50 coupler that divided the light into reference and sample arms. The backscattered lights from a reference mirror and a sample were combined to produce interference fringe pattern and collected by a line scan camera (SU1024-LDH2, Goodrich, Princeton NJ, USA) with 92 kHz line rate. The interference signal was presented as a function of wave-

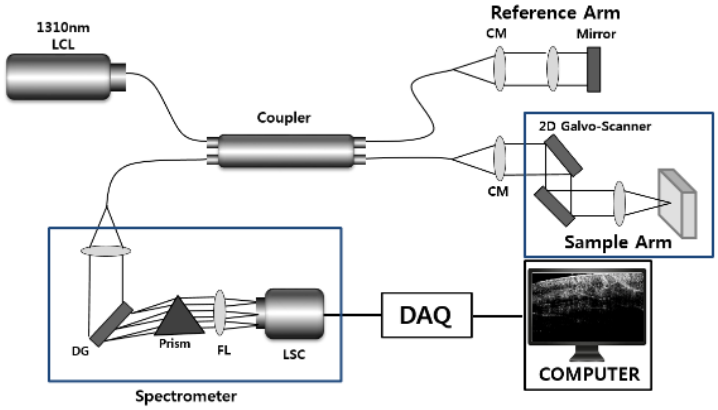

FIG. 1. Schematic diagram of 1310 nm k-linear OCT system. It is based on the Michelson interferometer. Broadband low coherent light was guided using an optical fiber to a 50:50 coupler that divided the light into reference and sample arms. The backscattered lights from a reference mirror and a sample were combined to produce interference fringe pattern and collected by a line scan camera. An equilateral triangular prism was inserted between a diffraction grating and a focusing lens in a spectrometer to linearize the diffraction angle of grating. CM: Collimator, DG: Diffraction Grating, FL: Focusing lens, LCL: Low coherence light source, LSC: Linear scan camera, DAQ: Data acquisition board.

number that was reduced to depth information using an inverse Fourier transform. Optical components in the sample and reference arms were designed to have the same fiber and free space lengths to minimize dispersion mismatch. An equilateral triangular prism was inserted between a diffraction grating and a focusing lens in a spectrometer to linearize diffraction angle of grating. From point spread function, we obtained an axial resolution of 11.692 μm in air, and a signal to noise ratio of 106 dB, a roll-off of 5.65 dB/mm to confirm the quality of our OCT system.

2.2 Optical coherence elastography setup

Optical coherence elastography was developed by combining the optical coherence tomography system with a mechanical loading system that located in the sample arm of OCT as shown in Fig. 2 [5, 9]. The loading system consisted of a stack of piezoelectric rings (NAC2124-H10-A01, Noliac Systems, Hardec Králové, Czech Republic), a glass plate tilted by 5 degree to prevent multiple reflection from the surface of glass plate (15 mm diameter × 1.5 mm thickness uncoated glass, Sukwang Precision Glass, Korea), and a silicone film (15 mm diameter × 600 μm thickness in center position, fabricated in the lab, called as reference phantom). The silicone film was attached at the bottom of the glass plate and made contact with the sample (tissue phantom). The reference phantom was used to monitor the amount of the applied force by deformation and the same reference phantom was used for all OCE measurements.

A stack of piezo-electric rings applied external force to the tissue phantom and the reference phantom. A pulse train of 200 voltage was applied to piezo-electric rings from

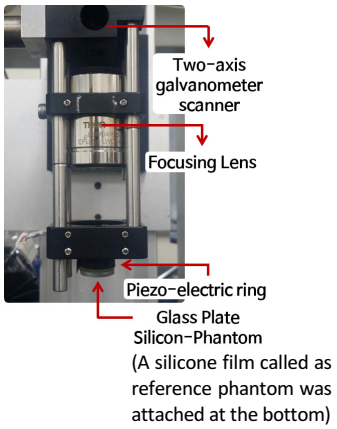

FIG. 2. Mechanical loading system attached in the sample arm (see Fig. 1). It consisted of a stack of piezoelectric rings, a glass plate (tilted by 5 degree to prevent multiple reflection from the surface of glass plate), and a silicone film (called as reference phantom). The silicone film was attached at the bottom of the glass plate and made contact with the sample (tissue phantom). The reference phantom was used to monitor the amount of the applied force by deformation and the same reference phantom was used for all OCE measurements.

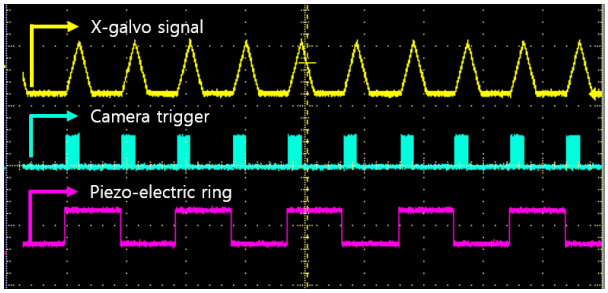

FIG. 3. Timing diagram to show synchronization among galvo-scanner, linear scan camera, and piezoelectric ring. Thousand twenty four A-line camera triggers were used to obtain a cross-sectional OCT image. The tissue phantoms were compressed when the piezo signal was high and released when the signal low. Two consecutive OCT images (with/without external loading) were acquired to be compared and to produce a displacement vector field.

piezo driver (NDR6220, Noliac Systems, Hardec Králové, Czech Republic). It was synchronized with the two-axis galvo-scanner and the line scan camera as shown in Fig. 3. A map of local strain was obtained by cross-correlation speckle tracking from two OCT images with/without external loading, respectively. A timing diagram to obtain two consecutive OCT images was provided in Fig. 3. OCT images were acquired when the signal for x-galvanometer (fast axis) was rising. A-line camera trigger was used. A cross-sectional image had 1024 A-lines that need the same number of A-line triggers. An on-off signal was applied to the piezoelectric ring. The phantoms were compressed when the signal was high and released when the signal low.

2.3 Fabrication of silicone phantoms

In order to test the feasibility of OCE for the measurement of tissue mechanical property, we, first, made silicone phantoms with similar optical and biomechanical properties to real tissues. Silicone phantoms were fabricated with pure polydimethylsiloxane (PDMS) fluid (50 cSt viscosity, Clearco Products Co., Inc., Willow Grove, PA, USA) and two curing agents (General Electric RTV-615 A and B, Circuit Specialists, Inc., Tempe, AZ, USA). Two groups of phantoms were prepared with different concentration ratio of three materials. The concentration ratio was indicated by the mass ratio among PDMS curing agent RTV-615 B, PDMS curing agent RTV-615 A, and pure PDMS fluid. It was 1:10:50 for phantom 1 and 1:10:30 for phantom 2. When the concentration of pure PDMS fluid increases, the number of cross-linking with RTV-615 curing agents decreases. Therefore, phantom 1 was expected to have a low elastic modulus. We made three phantoms per each group.

One milligram per gram of titanium dioxide (TiO_2) powder (Sigma-Aldrich, #224227, mean size 1 μm, <5 μm, St. Louis, MO, USA) was added to the mixture of phantom ingredient as an optical scattering particle for OCT imaging. In order to enhance dispersion of titanium dioxide, the

solution of phantom was mixed using an ultrasonicator for 1 hour at room temperature and vortexer. The solution was poured into an aluminum mold (20 mm × 20 mm × 20 mm) and cured at 90°C for 6 hours and at room temperature for 24 hours [10].

2.4 Compressive modulus measurement by rheometer

Rheometer has been used to measure mechanical properties of soft materials, for instance, jelly, tofu, breads, rubbers, capsules of medicines. In this study, compressive moduli of tissue phantoms were measured 3 times for each phantom by the rheometer (Compac-100II, Sun Science Co., Tokyo, Japan) with 2 kg load cell and averaged [11]. The speed of pressure sensitive shaft was 60 mm/min and the area of shaft head was 0.79 cm^2.

III. RESULTS AND DISCUSSION

3.1 Rheometer

The measured compressive modulus by the rheometer is shown in Fig. 4. Three phantoms were measured in each group. The averaged value for phantom 1 was 87.2387 kPa and phantom 2 was 197.9639 kPa. From this graph, we confirmed that phantom 1 was almost 2.3 times softer than phantom 2 due to the lack of cross-linking of PDMS. The error bars in Fig. 4 represent standard deviations that were 5.56 kPa and 31.14 kPa for phantom 1 and 2, respectively.

3.2 Optical coherence elastography

To estimate the strains of phantoms, two of optical coherence tomography images (with/without external loading) were acquired at the center of tissue phantoms as shown in Fig. 5(a). The reference phantom was inserted between glass plate and tissue phantom to monitor the amount of the applied force across all measurements. From these images, displacement vector field was acquired by cross-correlation speckle tracking using PIVlab Ver. 1.4 and was optimized to have best estimation by adjusting window and step size range (Fig. 5(b)). The optimized window size was 36 × 36 $pixels^2$ and step size was 4 × 4 $pixels^2$. Noise vectors were also removed manually. In the area with low speckle signal, interpolation was unavoidable due to missing data. The green arrows represent original data and the orange arrows interpolated data.

A map of local strain was calculated from the displacement vector image as shown in Fig. 5(c). The pixel size was adjusted to get 4 times larger than the pixel size of OCT image due to calculation of the displacement vector. Therefore the resolution of the local strain was 4 times worse than OCT resolution. The map of the local strain represents pseudo color indicating strain value at every location in the image. This map could represent local mechanical property of tissue if it was applied for diagnosis of disease in an early stage. The local strain does not have

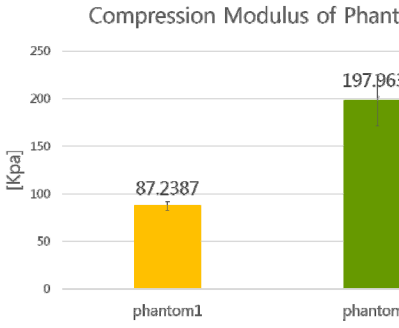

FIG. 4. Graph of compressive moduli of phantoms. Concentration ratios were 1:10:50 for phantom 1 and 1:10:30 for phantom 2 (PDMS curing agent RTV-615 B : PDMS curing agent RTV-615 A : pure PDMS fluid). Three phantoms were measured in each group.

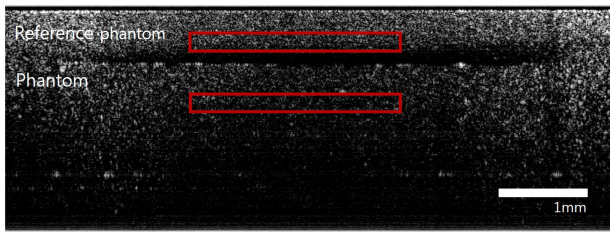

(a)

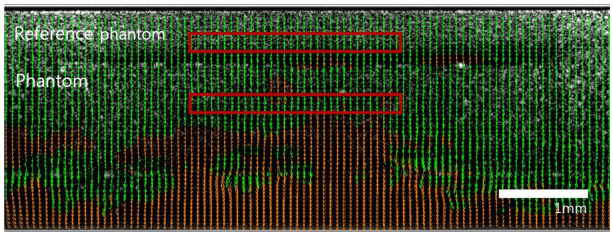

(b)

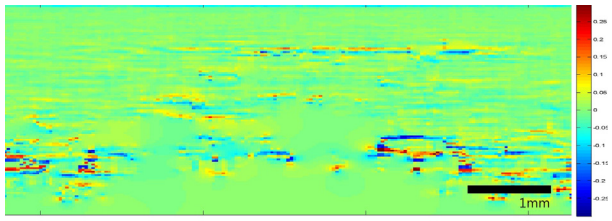

(c)

FIG. 5. (a) OCT image of reference phantom and phantom 1, (b) Displacement vector field (constructed from two consecutive OCT images using cross-correlation speckle tracking), (c) Local strain map of phantom. The optimized window size was set to 36 × 36 $pixels^2$ and step size to 4 × 4 $pixels^2$ to calculate the displacement vector in (b). In the area with low speckle signal, interpolation was unavoidable for missing data. The green arrows represent original data and the orange arrows interpolated data in (b). Local strain in (c) does not have a unit. It represents strain value at every location in the image. Negative value means compression and positive value elongation. Even if the local strain had positive values in some area, it mostly showed negative values as expected.

a unit. Negative value means compression and positive value elongation. The resolution of OCT was 11.7 μm which could result in uncertainty in displacement calculation by speckle tracking. Phantoms were made out of the mixture of PDMS, curing agents, and TiO2. High viscosity of pure PDMS might result in some degree of inhomogeneity. These two might cause positive values in the local strain. Even if the local strain had positive values in some area, it mostly showed negative values as expected.

Axial displacements of the tissue phantom and the reference phantoms were acquired in the subarea (red boxes in Fig. 5(b)) at the center of the displacement vector images. They were averaged along horizontal direction in the subarea to plot a graph of axial displacement versus depth as shown in Fig. 6. The slopes of trend lines represent strain values by Eq. (3). Red, yellow, blue, and green trend lines are corresponding to four strains which are denoted as ε_r^1, ε_1, ε_r^2, and ε_2, respectively. The subscripts indicate different materials. r, for example, is for the reference phantom, 1 is for the tissue phantom 1, and 2 is for the tissue phantom 2. The superscripts mean loading number. Note that the same reference phantom was used for loading 1 and 2. The tissue phantom 1 and the reference phantom were under the same stress by loading 1. The tissue phantom 2 and the reference phantom were under the same stress by loading 2. The four strain values were all we needed to know stiffness ratio of the tissue phantom 2 to 1. It is the beauty of this study using the reference phantom by noting that OCE is based on displacement (not force) measurement. Detailed derivation is as follows.

From Eq. (1), the compressive moduli of the tissue phantom 1, 2, and the reference phantom can be written as

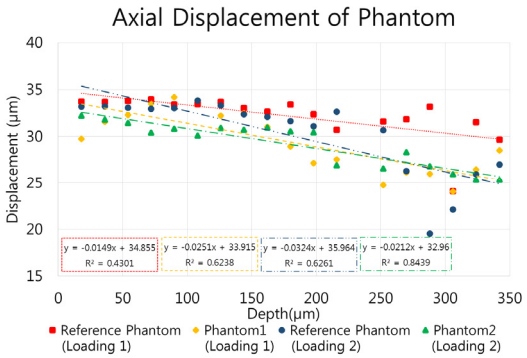

FIG. 6. Graph of axial displacements of the tissue phantoms and the reference phantom. They were averaged along horizontal direction in the subarea (red boxes) in Fig. 5(b). The slope of trend line representing axial strain was obtained from linear regression. The coefficient of determination (R^2) was provided along with fitting equation. 95% confidence interval and p-value for the slope were given in Table 1. Four slopes were used to calculate stiffness ratio of the tissue phantom 2 to 1.

$$Y_1 = \sigma_1/\varepsilon_1 \tag{4}$$

$$Y_2 = \sigma_2/\varepsilon_2 \tag{5}$$

$$\text{and} \quad Y_r = \sigma_1/\varepsilon_r^1 = \sigma_2/\varepsilon_r^2, \text{ respectively.} \tag{6}$$

From Eq. (6),

$$\sigma_1/\sigma_2 = \varepsilon_r^1/\varepsilon_r^2 \tag{7}$$

By Eq. (7), the stiffness ratio, therefore, can be represented as

$$\frac{Y_2}{Y_1} = \frac{\sigma_2/\varepsilon_2}{\sigma_1/\varepsilon_1} = \frac{\sigma_2/\sigma_1}{\varepsilon_2/\varepsilon_1} = \frac{\varepsilon_r^2/\varepsilon_r^1}{\varepsilon_2/\varepsilon_1} \tag{8}$$

By Eq. (8), we found that the tissue phantom 1 is almost 2.6 times softer than phantom 2. This result was summarized in Table 1 and closely matched with the rheometer measurement. Relatively low R^2 (coefficient of determination) in Fig. 6 were attributed to the same two causes: phantom inhomogeneity and uncertainty in displacement calculation. 95% confidence interval and p-value for the slope in Fig. 6 were provided in Table 1.

On the other hand, by using Eq. (4)-(6),

$$Y_r = Y_1\,\varepsilon_1/\varepsilon_r^1 = Y_2\,\varepsilon_2/\varepsilon_r^2 \tag{9}$$

The compressive modulus of the reference phantom Y_r can be calculated from Eq. (9) if we use the rheometer measurement for Y_1 or Y_2. The compressive modulus of the reference phantom was 146.95 kPa or 129.53 kPa, respectively. The compressive modulus of the reference phantom could not be measured by the rheometer because its thickness (600 μm) was much thinner than minimum measurable thickness (20 mm) of the rheometer. If we can obtain reliable value of Y_r, OCE developed in this study can estimate the absolute stiffness like the rheometer (Eq. (9) gives us Y_1 and Y_2 separately). With the given Y_r, one can calculate surface force at the top surface of the reference phantom from the local strain (measured by OCE). The surface force is what the load cell measures in the rheometer. Therefore, the rheometer performs the same thing as what OCE does. Note that OCE and rheometer are limited in that both need a model for the sample or need to predict the internal local stress without much error from the surface force. OCE, however, has an advantage over the rheometer. OCE can provide local strain and that is what the rheometer cannot do.

In this study, we assumed that the samples exhibited isotropic, linear, and elastic characteristics. Most of biological samples are generally anisotropic, nonlinear, and/or viscoelastic. Muscle, for instance, has many fibers aligned

TABLE 1. Strain values measured by OCE and stiffness ratio of two tissue phantoms

	Loading 1		Loading 2		The stiffness ratio (-) of phantom 2 to 1, Y_2/Y_1 (Eq. (8))
	Strain (-) of the reference phantom, ε_r^1	Strain (-) of the tissue phantom 1, ε_1	Strain (-) of the reference phantom, ε_r^2	Strain (-) of the tissue phantom 2, ε_2	
Slope	-0.0149	-0.0251	-0.0324	-0.0212	2.58
95% confidence interval for the slope (Maximum)	-0.0058	-0.0147	-0.0191	-0.0163	
95% confidence interval for the slope (Minimum)	-0.0240	-0.0354	-0.0456	-0.0260	
p-value for the slope	0.0031	0.000097	0.000092	0.000000075	

in one direction and shows anisotropy. In this case, the generalized Hooke's law might be used which is the most general linear relation among all the components of the stress and strain tensor. In a simplified model, skin tends to have nonlinearity. In order to apply the analysis done here to nonlinear samples, special attention should be paid. The stiffness of nonlinear sample varies with preload and magnitude of applied force. In the uniaxial compression, the preload is inevitable to keep a loading actuator in contact with the sample and make sure the force is fully exerted in the axial direction. If linearity cannot be assumed, the preload may affect the distribution of internal forces induced by the applied force (for example, by changing the effective stiffness of the material). Therefore, if one wants to compare the stiffnesses of two different nonlinear samples, the preload should be the same. In this case, the deformation of the reference phantom by the preload has to be the same across all measurements.

IV. CONCLUSION

In this study, we developed an optical coherence elastography system with a mechanical loading system and a deformation-based force indicator (the reference phantom). Silicone tissue phantoms were fabricated to mimic biomechanical and optical properties of real tissue. The mechanical property of tissue phantom was measured by a rheometer and an optical coherence elastography system to be compared with each other. From these results, we confirmed the possibility of optical coherence elastography as a biomedical modality to measure mechanical property of tissue. Accuracy and repeatability of optical coherence elastography need to be studied more in the future.

ACKNOWLEDGMENT

This work was supported by a Research Grant of Pukyong National University (2015 year).

REFERENCES

1. B. F. Kennedy, K. M. Kennedy, and D. D. Sampson, "A Review of Optical Coherence Elastography: Fundamentals, Techniques and Prospects", IEEE Journal of Selected Topics in Quantum Electronics **20**, 2, 272-288, 2014.
2. K. J. Parker, M. M. Doyley, and D. J. Rubens, "Imaging the elastic properties of tissue : the 20 year perspective", Physics in Medicine and Biology, **56**, R1-R29, 2011
3. Y. K. Mariappan, K. J Glaser, and R. L. Ehman, "Magnetic resonance elastography: A review", Clinical Anatomy, **23**, 497-511, 2010.
4. X. Liang, V. Crecea, and S. A. Boppart, "Dynamic optical coherence elastography: A review", Journal of innovative optical health sciences, **3**, 4, 221-233, 2010.
5. B. F. Kennedy, X. Liang, S. G. Adie, D. K. Gerstmann, B. C. Quirk, S. A. Boppart, and D. D. Sampson, "In vivo three-dimensional optical coherence elastography", Optics Express, **19**, 6623-6634, 2011.
6. M. M. Doyley, "Model-based elastography: a survey of approaches to the inverse elasticity problem," Phys. Med. Biol., **57** (3), R35-R73, 2012.
7. W. Drexler, "Ultrahigh-resolution optical coherence tomography", Journal of Biomedical Optics, **9**, 47-74, 2004.
8. V. M. Gelikonov, G. V. Gelikonov, and P. A. Shilyagin, "Linear-Wavenumber Spectrometer for High-Speed Spectral-Domain Optical Coherence Tomography", Optics and Spectroscopy, **106**, 459-465, 2009.
9. J. M. Schmitt, "OCT elastography: imaging microscopic deformation and stain of tissue", Optics Express, **3**, 199-211, 1998.
10. X. Liang, A. L. Oldenburg, V. Crecea, E. J. Chaney, and S. A. Boppart, "Optical micro-scale mapping of dynamic biomechanical tissue properties", Optics Express, **16**, 11052-11065, 2008.
11. Y. Gui, S. K. Gil, and G. H. Ryu, "Effects of extrusion condition on the physicochemical properties of extruded red ginseng", Preventive Nutrition and Food Science, **17**, 203-209, 2012.